JHEP

Published for SISSA by Springer

Received: March 24, 2020
Accepted: April 23, 2020
Published: May 12, 2020

CP violation from τ, t and b dimension-6 Yukawa couplings — interplay of baryogenesis, EDM and Higgs physics

Elina Fuchs,[a,b,c] **Marta Losada,**[d] **Yosef Nir**[a] **and Yehonatan Viernik**[a]

[a] *Department of Particle Physics and Astrophysics, Weizmann Institute of Science, Rehovot 7610001, Israel*

[b] *Fermilab, Theory Department, Batavia, IL 60510, U.S.A.*

[c] *Department of Physics, University of Chicago, Chicago, IL 60637, U.S.A.*

[d] *New York University Abu Dhabi, PO Box 129188, Saadiyat Island, Abu Dhabi, United Arab Emirates*

E-mail: elinafuchs@uchicago.edu, marta.losada@nyu.edu, yosef.nir@weizmann.ac.il, yehonatan.viernik@weizmann.ac.il

Abstract: We explore the implications of the Standard Model effective field theory (SMEFT) with dimension-six terms involving the Higgs boson and third-generation fermion fields on the rate of Higgs boson production and decay into fermions, on the electric dipole moments (EDMs) of the electron, and on the baryon asymmetry of the Universe. We study the consequences of allowing these additional terms for each flavor separately and for combinations of two flavors. We find that a complex τ Yukawa coupling can account for the observed baryon asymmetry $Y_B^{\rm obs}$ within current LHC and EDM bounds. A complex b (t) Yukawa coupling can account for 4% (2%) of $Y_B^{\rm obs}$, whereas a combination of the two can reach 12%. Combining τ with either t or b enlarges the viable parameter space owing to cancellations in the EDM and in either Higgs production times decay or the total Higgs width, respectively. Interestingly, in such a scenario there exists a region in parameter space where the SMEFT contributions to the electron EDM cancel and collider signal strengths are precisely SM-like, while producing sufficient baryon asymmetry. Measuring CP violation in Higgs decays to τ leptons is the smoking gun for this scenario.

Keywords: Cosmology of Theories beyond the SM, CP violation, Higgs Physics

ArXiv ePrint: 2003.00099

Open Access, © The Authors.
Article funded by SCOAP[3].

https://doi.org/10.1007/JHEP05(2020)056

JHEP05(2020)056

Contents

JHEP05(2020)056

1 Introduction

The first decade of the LHC experiments led to significant progress in our understanding of Nature. Two very important aspects of this progress have been the following:

- A new scalar particle has been discovered [1, 2] with properties that fit, within present experimental accuracy, to those of the Standard Model (SM) Higgs boson [3–8].
- No other new elementary particles have been discovered, with lower bounds on the mass of large classes of such hypothetical particles at the TeV scale [9, 10].

This situation makes it plausible that the scale of new physics is high enough above the electroweak scale that its effects can be parameterized via higher-dimension operators, and motivates an interpretation of experimental results in the framework of the Standard Model effective field theory (SMEFT). The Higgs program provides a unique window into various classes of such higher-dimension terms in the Lagrangian.

We are particularly interested in dimension-six operators [11, 12] that couple the Higgs boson field to fermion fields. The presence of these additional terms provides two important features: novel CP-violating interactions [13] and violation of the SM relation between the fermion mass and its Yukawa coupling. These features lead to interesting consequences:

- Modifications to the Higgs production and decay rates, which can potentially be discovered by collider experiments;
- New contributions to the electric dipole moment of the electron (EDM), potentially within present or near-future reach of experiments;
- New contributions to the baryon asymmetry via electroweak baryogenesis (EWBG), with the potential of opening a window to solving this long-standing problem.

In this work we study these effects and their interplay for the fermions of the third generation, τ, b and t. The details and implications for the muon can be found in ref. [14]. For previous work on the possible role of third-generation fermions in the aspect of CP violation for EWBG, see e.g. refs. [13, 15] for quarks, and refs. [16, 17] for the tau-lepton. Real dim-6 Yukawas of the t and b were constrained by earlier Run-2 LHC data in ref. [18]. EDM and Run-1 LHC constraints on complex dim-6 couplings were considered in ref. [19].

This paper is organized as follows. In section 2 we introduce our theoretical framework and a useful parameterization of the coupling constants. Sections 3 and 4 present the effect of the dimension-six terms on electroweak baryogenesis and the electron EDM, respectively. We then focus in section 5 on the LHC results of Higgs boson decay rates to fermion pairs and vector boson pairs from various production channels, as well as on the modifications of the total Higgs width. We derive the constraints these measurements impose on the new physics captured in the dimension-six terms. Sections 6.1 and 6.2 present our results for single species and for combinations of two fermions. In section 7 we summarize and present our conclusions.

JHEP05(2020)056

2 Dimension-six complex Yukawa terms

We consider the following dimension-four and dimension-six Yukawa-type Lagrangian terms for the third-generation fermions (similarly to refs. [13, 17], but allowing also for a real part of the dimension-six term):

$$\mathcal{L}_{\rm Yuk} = y_f \overline{F_L} F_R H + \frac{1}{\Lambda^2}\left(X_R^f + iX_I^f\right)|H|^2 \overline{F_L} F_R H + \text{h.c.} \tag{2.1}$$

Here F_L is the SU(2)-doublet field containing $F = t, b, \tau$, F_R is the corresponding SU(2)-singlet field, H is the Higgs doublet field, and Λ is the mass scale of new physics. Without loss of generality, we take y_f to be real. Substituting in the unitary gauge

$$H = \frac{1}{\sqrt{2}}(v + h), \tag{2.2}$$

leads to the following mass term and h-Yukawa couplings:

$$\begin{aligned}\mathcal{L}_f = {} & \frac{y_f v}{\sqrt{2}}\left[1 + \frac{v^2}{2\Lambda^2}\frac{X_R^f + iX_I^f}{y_f}\right]\overline{f_L} f_R + \frac{y_f}{\sqrt{2}}\left[1 + \frac{3v^2}{2\Lambda^2}\frac{X_R^f + iX_I^f}{y_f}\right]\overline{f_L} f_R h \\ & + \frac{3v}{2\sqrt{2}\Lambda^2}\left(X_R^f + iX_I^f\right)\overline{f_L} f_R hh + \frac{1}{2\sqrt{2}\Lambda^2}\left(X_R^f + iX_I^f\right)\overline{f_L} f_R hhh.\end{aligned} \tag{2.3}$$

We define the ratio of the dim-6 to the dim-4 contribution to a fermion mass as our useful coordinates to be used in the following:

$$T_R^f \equiv \frac{v^2}{2\Lambda^2}\frac{X_R^f}{y_f}, \quad T_I^f \equiv \frac{v^2}{2\Lambda^2}\frac{X_I^f}{y_f}. \tag{2.4}$$

Thus the coefficients of the mass and Yukawa terms in eq. (2.3) have the following values:

$$m_f = \frac{y_f v}{\sqrt{2}}\left(1 + T_R^f + iT_I^f\right), \quad \lambda_f = \frac{y_f}{\sqrt{2}}\left(1 + 3T_R^f + 3iT_I^f\right). \tag{2.5}$$

Once we add the dimension-six terms, we are no longer in the basis of real fermion masses. To have m_f real in the $m_f \overline{f_L} f_R$ term, we transform $f_R \to e^{i\theta_f} f_R$ by θ_f which satisfies

$$\tan\theta_f = \frac{T_I^f}{1 + T_R^f}. \tag{2.6}$$

Then, in the mass basis with a real value for the mass,

$$m_f = \frac{y_f v}{\sqrt{2}}\sqrt{\left(1 + T_R^f\right)^2 + T_I^{f2}}, \tag{2.7}$$

we have the following Yukawa coupling:

$$\lambda_f = \frac{y_f}{\sqrt{2}}\frac{1 + 4T_R^f + 3T_R^{f2} + 3T_I^{f2} + 2iT_I^f}{\sqrt{(1 + T_R^f)^2 + T_I^{f2}}}. \tag{2.8}$$

JHEP05(2020)056

The dim-4 coupling y_f can be written in terms of T_R^f, T_I^f via the expression (2.7) for the mass. In turn, this can be related to the SM Yukawa coupling via

$$\left(\frac{y_f}{y_f^{\rm SM}}\right)^2 = \frac{1}{\left(1+T_R^f\right)^2 + T_I^{f2}}\,. \tag{2.9}$$

Thus, the full setup of eq. (2.1) is described by two free parameters per fermion, T_R^f and T_I^f.

3 The baryon asymmetry Y_B

The value of the baryon asymmetry is extracted from CMB measurements. It is given by $\Omega_b h^2 = 0.02226(23)$ [20] or, equivalently,

$$Y_B^{\rm obs} = (8.59 \pm 0.08) \times 10^{-11}. \tag{3.1}$$

Electroweak baryogenesis is the mechanism through which a non-zero value of the baryon number density is obtained during the electroweak phase transition (EWPT). As bubbles expand to fill the universe with the non-zero vacuum expectation value of the Higgs field, CP-violating interactions across the bubble wall create a chiral asymmetry, which is then converted to a baryon asymmetry by the weak sphaleron process. Electroweak baryogenesis requires two ingredients that go beyond the SM:

- New sources of CP violation [21, 22];
- Modification of the EWPT such that it is strongly first order (rather than a smooth crossover, as is the case in the SM [23, 24]).

In this work we focus on the aspect of CP violation. We thus make the following assumptions regarding the EWPT:

- There are additional degrees of freedom that lead to a strongly first-order EWPT;
- These additional degrees of freedom do not significantly affect the interactions of the SM fermion fields across the expanding bubble wall;
- There are no additional sources of CP violation from the interactions of these degrees of freedom that would significantly modify the resulting value of the baryon asymmetry.

3.1 Particle dynamics

We calculate the final matter-antimatter asymmetry in the Closed Time Path formalism, following [13, 17, 25, 26]. For simplicity, we provisionally consider the case that only one active fermion species with a non-zero dimension-six term provides a source for generating the asymmetry. Here we neglect first and second lepton generations due to the smallness of their Yukawa couplings (for muon-driven EWBG see ref. [14]). Interactions of light quarks are neglected as well, but they participate in the strong sphaleron process, which is fast

JHEP05(2020)056

at high temperatures. Gauge interactions are fast enough to be considered in equilibrium. The dimension-six term leads to both CP-odd and CP-even processes that compete to produce and wash out a CP asymmetry. The summary of the process is as follows:

- CP-violating interactions across the expanding bubble wall generate a chiral asymmetry, while CP-conserving interactions wash out the generated asymmetry.
- The strong sphaleron process produces further washout in the quark sector.
- Some of the remaining asymmetry diffuses into the symmetric phase. Diffusion is dominantly affected by gauge interactions, hence it is more efficient for leptons than for quarks.
- The weak sphaleron process is efficient only in the symmetric phase, acting on left-handed multiplets and changing baryon number.
- The chemical potential due to the chiral asymmetry induces a preferred direction for the weak sphaleron, thus generating a baryon asymmetry.
- Finally, the bubble wall catches up and freezes in the resulting baryon number density in the broken phase.

The full dynamics described above is encoded in a coupled set of differential equations, the transport equations, one for each flavor f:

$$\partial_\mu f^\mu = -\Gamma^f_M \mu^f_M - \Gamma^f_Y \mu^f_Y + \Gamma^f_{\rm ss}\mu_{\rm ss} - \Gamma^f_{\rm ws}\mu^f_{\rm ws} + S_f, \tag{3.2}$$

where the relaxation and Yukawa rates Γ^f_M, Γ^f_Y relate to CP-conserving interactions; the strong sphaleron rate $\Gamma_{\rm ss}$ is non-zero only for quarks; and the weak sphaleron rate $\Gamma^f_{\rm ws}$ is non-zero only for left-handed fermions. A chemical potential μ is associated with each of these processes, and S_f is the CP-violating source, which does not admit a chemical potential. The method we used to solve this set of equations and other details are presented in [27].

3.2 Impact of T_R and T_I

The baryon asymmetry is proportional to the source, $Y_B \propto S \propto T_I$ at lowest order. Hence the T_R dependence enters only from second order in $T_{R,I} \propto 1/\Lambda^2$ onward, thus at $\mathcal{O}(1/\Lambda^4)$.[1]

In addition to the dependence of the CP violation source S_f on the dimension-six terms,

$$S_f \propto \mathcal{I}m(m^*_f m'_f) \propto y^2_f T^f_I, \tag{3.3}$$

[1] At $\mathcal{O}(1/\Lambda^4)$, there are contributions from both dim-6 terms squared and dim-4 times dim-8 terms. The contribution from the former is, however, enhanced by $1/y_f$ compared to the latter, and therefore, for the b-quark and for the τ-lepton, the latter can be neglected. For the effects of dim-8 terms on Y_B from a complex t-Yukawa, see ref. [13].

JHEP05(2020)056

the relaxation rate Γ_M, which originates from two mass insertions, and the Yukawa rate Γ_Y, which originates from two Yukawa insertions, are rescaled by T_R^f, T_I^f-dependent factors:

$$\Gamma_M \to \left[\frac{(1+r_{N0}^2 T_R^f)^2 + r_{N0}^2 T_I^{f2}}{(1+T_R^f)^2 + T_I^{f2}}\right]\Gamma_M\,,$$
$$\Gamma_Y \to \left[\frac{(1+3r_{N0}^2 T_R^f)^2 + (3r_{N0}^2 T_I^f)^2}{(1+T_R^f)^2 + T_I^{f2}}\right]\Gamma_Y\,. \tag{3.4}$$

Here $r_{N0} \equiv v(T=T_N)/v(T=0)$, where T_N is the nucleation temperature.

Our numerical calculation yields, to leading order[2] in T_I, T_R, for $T_R = 0$ and parameters as in appendix B and [27],

$$Y_B = 8.6\times 10^{-11}\times\left(51T_I^t - 23T_I^\tau - 0.44T_I^b\right). \tag{3.5}$$

We learn that the relevant range for each of the third generation fermions to account for the baryon asymmetry is

$$|T_I^t| = \mathcal{O}(0.02), \quad |T_I^\tau| = \mathcal{O}(0.04), \quad |T_I^b| > 1. \tag{3.6}$$

4 The electron EDM d_e

An upper bound on the electric dipole moment of the electron $|d_e|$ was recently obtained by the ACME collaboration [28]:

$$|d_e^{\max}| = 1.1\times 10^{-29}\ e\ \text{cm at } 90\%\,\text{C.L.}. \tag{4.1}$$

The dimension-six terms contribute also to d_e. We rewrite the relevant results obtained in ref. [29] in terms of our parameterization. The finite contributions from the Barr-Zee diagrams are given by

$$\frac{d_e^{(t)}}{e} \simeq -\frac{16}{3}\frac{e^2}{(16\pi^2)^2}\frac{m_e}{m_t}\frac{v}{\Lambda^2}X_I^t\left(2+\ln\frac{m_t^2}{m_h^2}\right), \tag{4.2}$$
$$\frac{d_e^{(b)}}{e} \simeq -4N_c Q_b^2\frac{e^2}{(16\pi^2)^2}\frac{m_e m_b}{m_h^2}\frac{v}{\Lambda^2}X_I^b\left(\frac{\pi^2}{3}+\ln^2\frac{m_b^2}{m_h^2}\right),$$
$$\frac{d_e^{(\tau)}}{e} \simeq -4Q_\tau^2\frac{e^2}{(16\pi^2)^2}\frac{m_e m_\tau}{m_h^2}\frac{v}{\Lambda^2}X_I^\tau\left(\frac{\pi^2}{3}+\ln^2\frac{m_\tau^2}{m_h^2}\right).$$

Working in the real mass basis and using the full Yukawa interaction (2.8), the sum of the t, b, τ finite contributions becomes

$$\frac{d_e}{e} \simeq -\frac{32\sqrt{2}}{3}\frac{e^2}{(16\pi^2)^2}\frac{m_e}{v^2}\left[\left(2+\ln\frac{m_t^2}{m_h^2}\right)\left(\frac{y_t}{y_t^{\rm SM}}\right)^2 T_I^t\right. \tag{4.3}$$
$$\left. +\frac{1}{4}\left(\frac{\pi^2}{3}+\ln^2\frac{m_b^2}{m_h^2}\right)\frac{m_b^2}{m_h^2}\left(\frac{y_b}{y_b^{\rm SM}}\right)^2 T_I^b + \frac{3}{4}\left(\frac{\pi^2}{3}+\ln^2\frac{m_\tau^2}{m_h^2}\right)\frac{m_\tau^2}{m_h^2}\left(\frac{y_\tau}{y_\tau^{\rm SM}}\right)^2 T_I^\tau\right].$$

[2] For large T_I, T_R, the dependence via eq. (2.9) will become relevant.

JHEP05(2020)056

Hence, the leading dim-6 dependence is on T_I^f, but through $(y_f/y_f^{\rm SM})$ given in eq. (2.9) also on T_R^f:

$$d_e \approx 1.1\times10^{-29}\, e\,\text{cm} \times \left[2223\left(\frac{y_t}{y_t^{\rm SM}}\right)^2 T_I^t + 9.6\left(\frac{y_\tau}{y_\tau^{\rm SM}}\right)^2 T_I^\tau + 11.6\left(\frac{y_b}{y_b^{\rm SM}}\right)^2 T_I^b\right]. \tag{4.4}$$

We learn that for $y_f = \mathcal{O}(y_f^{\rm SM})$, the sensitivity of the current searches for d_e is

$$T_I^t = \mathcal{O}(0.0004), \quad T_I^\tau = \mathcal{O}(0.1), \quad T_I^b = \mathcal{O}(0.09). \tag{4.5}$$

Additional constraints arise from measurements of the electric dipole moments of the neutron, mercury or thalium, see refs. [19, 30, 31] and references therein. However, both the hadronic and matrix element uncertainties, and possible cancellations [32] from CP-odd contributions involving the top and/or the bottom quark to these observables via Barr-Zee diagrams, the Weinberg operator, chromo-electric dipole moments for light quarks etc., make the constraints on $T_I^{t,b}$ weaker. In the case of a nonzero T_I^τ, there is only a Barr-Zee type contribution to the neutron EDM. However, given the current experimental upper bound on the neutron EDM [33], it does not provide a stronger constraint on T_I^τ.

5 Higgs production and decay

In this section, we derive the dependence of Higgs production and decay rates on T_R and T_I for cases where either one or two Yukawa couplings of third generation fermions are modified by dim-6 contributions. We then present those collider processes that are most sensitive to the considered coupling modifications, and their current experimental bound. In order to obtain the strongest available bound from Run-2 data, we combine the published values of ATLAS and CMS in a naive theorists' approach as the weighted mean with symmetric upper and lower uncertainties. The details of individual rates and their underlying data sets are summarized in appendix A.1.

5.1 Signal strength

The Higgs signal strength of production mode I (such as $I = \text{ggF}$) and decay channel into a final state F is defined as

$$\mu_I^F \equiv \frac{\sigma_I(pp\to h)\cdot\Gamma(h\to F)/\Gamma_h}{[\sigma_I(pp\to h)\cdot\Gamma(h\to F)/\Gamma_h]_{\rm SM}}, \tag{5.1}$$

where Γ_h is the total Higgs width. To extract the dependence of μ_I^F on the SMEFT parameters, it is convenient to define the dimensionless parameters r_f:

$$r_f \equiv \frac{|\lambda_f|^2/|\lambda_f^{\rm SM}|^2}{|m_f|^2/|m_f^{\rm SM}|^2} = \frac{(1+3T_R^f)^2+9T_I^{f2}}{(1+T_R^f)^2+T_I^{f2}}\,. \tag{5.2}$$

JHEP05(2020)056

5.1.1 Production rates

The main production modes of the discovered Higgs boson at $m_h = 125\,\text{GeV}$ are gluon fusion (ggF), associated $t\bar{t}h$ and th production (together denoted as tth), vector-boson associated production (Vh, $V = Z, W$) and vector-boson fusion (VBF). The ggF and tth production rates are proportional to $|\lambda_t|^2$ (neglecting the very small b quark contribution), whereas the Vh and VBF rates do not depend on any Yukawa coupling:

$$\begin{aligned} \sigma_{\text{ggF}}/\sigma_{\text{ggF}}^{\text{SM}} &= \sigma_{tth}/\sigma_{tth}^{\text{SM}} = r_t, \\ \sigma_{Vh}/\sigma_{Vh}^{\text{SM}} &= \sigma_{\text{VBF}}/\sigma_{\text{VBF}}^{\text{SM}} = 1. \end{aligned} \tag{5.3}$$

5.1.2 Decay rates

We consider modifications of decays into fermion pairs $F = \bar{f}f$. We obtain:

$$\Gamma(h \to f\bar{f})/[\Gamma(h \to f\bar{f})]^{\text{SM}} = r_f \quad (f = b, \tau). \tag{5.4}$$

We also make use of decays into the weak vector-bosons:

$$\Gamma(h \to VV^*)/[\Gamma(h \to VV^*)]^{\text{SM}} = 1 \quad (V = W, Z). \tag{5.5}$$

5.1.3 The total Higgs width

Within our framework, the total Higgs width is affected by modification of λ_b, via $\Gamma(h \to b\bar{b})$ with SM branching ratio $\text{BR}_b^{\text{SM}} = 0.58$, by modification of λ_τ, via $\Gamma(h \to \tau^+\tau^-)$ with $\text{BR}_\tau^{\text{SM}} \sim 0.063$, and by modification of λ_t, via $\Gamma(h \to gg)$ with $\text{BR}_g^{\text{SM}} \sim 0.086$ [34]:

$$\Gamma_h/\Gamma_h^{\text{SM}} = 1 + \text{BR}_b^{\text{SM}}(r_b - 1) + \text{BR}_\tau^{\text{SM}}(r_\tau - 1) + \text{BR}_g^{\text{SM}}(r_t - 1)\,, \tag{5.6}$$

where we neglect the modification of the total width by the λ_t-induced change of $h \to \gamma\gamma$ due to the small $\text{BR}_\gamma^{\text{SM}} \sim 0.002$. The total width is constrained as $0.08\,\text{MeV} \leq \Gamma_h \leq 9.16\,\text{MeV}$ at 95% C.L.by CMS [35], assuming an SM-like coupling structure, which applies in the considered framework. The SM prediction is $\Gamma_h^{\text{SM}} = 4.1\,\text{MeV}$.

5.2 Single-flavor modification

Consider the case that a single Yukawa coupling λ_f is modified. For $\mu_f \neq \hat{\mu}_f$ with

$$\hat{\mu}_f \equiv \frac{9}{1 + 8\text{BR}_f^{\text{SM}}}\,, \tag{5.7}$$

the expression for the signal strength

$$\mu_f = \frac{r_f}{1 + \text{BR}_f^{\text{SM}}(r_f - 1)} \tag{5.8}$$

defines a circle in the (T_R, T_I) plane

$$T_I^{f\,2} + (T_R^f - T_{R0}^f)^2 = R_T^2\,, \tag{5.9}$$

JHEP05(2020)056

centered at $(T_R^f, T_I^f) = (T_{R0}^f, 0)$, and with radius R_T,[3]

$$\begin{aligned} T_{R0}^f &= -\frac{3-\mu_f\,(1+2\mathrm{BR}_f^{\mathrm{SM}})}{9-\mu_f\,(1+8\mathrm{BR}_f^{\mathrm{SM}})}\,, \\ R_T^2 &= \frac{4\mu_f\,(1-\mu_f\,\mathrm{BR}_f^{\mathrm{SM}})(1-\mathrm{BR}_f^{\mathrm{SM}})}{\left[9-\mu_f\,(1+8\mathrm{BR}_f^{\mathrm{SM}})\right]^2}\,. \end{aligned} \tag{5.10}$$

Thus, for a given $\mathrm{BR}_f^{\mathrm{SM}}$, only a certain range of μ_f yields a real solution:

$$\mu_f \leq \frac{1}{\mathrm{BR}_f^{\mathrm{SM}}}\,. \tag{5.11}$$

It is interesting to note that, even for $\mu_f = 1$, there exist solutions other than the trivial $T_R^f = T_I^f = 0$ one, and they are independent of $\mathrm{BR}_f^{\mathrm{SM}}$: $T_{R0}^f = -1/4$ and $R_T^f = 1/4$ such that

$$T_I^{f2} = -\frac{1}{2}T_R^f - T_R^{f2}. \tag{5.12}$$

Thus, even if experiments close in on $\mu_f = 1$, there will be an allowed circle in the (T_R^f, T_I^f) plane. In particular, a new source of CP violation, $T_I^f \neq 0$ (with $|T_I^f| \leq 1/4$), will be allowed. An experimental range, $\mu^{\min} \leq \mu \leq \mu^{\max}$, translates into an allowed region between two circles in this plane.

5.2.1 λ_τ

The Yukawa coupling λ_τ is constrained by measurements of $\mu_{\tau^+\tau^-}$. If only the τ Yukawa coupling is modified by dim-6 terms, then only $\Gamma(h \to \tau^+\tau^-)$ and Γ_h are modified from their SM predictions. One can therefore combine the measurements of all Higgs production modes with the Higgs decaying into a pair of tau-leptons (for further details, see table 2):

$$\mu_{\tau^+\tau^-} = 0.91 \pm 0.13. \tag{5.13}$$

Using eq. (5.8) for $f = \tau$ where r_τ is defined in eq. (5.2), we find that both the upper and lower 2σ-bounds yield a circle in the (T_R^τ, T_I^τ) plane, resulting in the LHC-allowed ring shown in figure 1.

5.2.2 λ_b

The Yukawa coupling λ_b is constrained by measurements of $\mu_{b\bar{b}}$ via eq. (5.8) for $f = b$. Neglecting the 1% bottom loop contribution to ggF, we combine all available production modes with the subsequent decay of $h \to b\bar{b}$ (see table 2) as

$$\mu_{b\bar{b}} = 1.02 \pm 0.14\,, \tag{5.14}$$

which is dominated by μ_{Vh}^{bb}.

[3] In the vicinity of $\hat{\mu}_f$, the radius gets very large. Precisely at that value, the solutions of (5.8) become independent of T_I^f, namely $T_R = -2/3$, or $\mathrm{BR}_f^{\mathrm{SM}} = 1$. However, such values are excluded by more than 3σ by the bounds of eqs. (5.13)–(5.15).

JHEP05(2020)056

σ_I	$\Gamma(h \to F)$	Γ_h	f_1, f_2	process	dependence
SM	f_1	f_1, f_2	τ, b	any production, $h \to \tau\tau, b\bar{b}$	A: eq. (5.16)
			t, τ	Vh+VBF, $h \to \tau\tau$	
			t, b	Vh+VBF, $h \to b\bar{b}$	
f_1	SM	f_1, f_2	$t, b/\tau$	ggF+tth, $h \to VV$	
f_1	f_2	f_1, f_2	t, τ	ggF+tth, $h \to \tau\tau$	B: eq. (5.17)
			t, b	ggF+tth, $h \to b\bar{b}$	

Table 1. Possible modifications of the signal strengths μ_I^F for two modified Yukawa couplings of the fermions f_1, f_2. The Higgs production cross section σ_I, with $I = Vh$+VBF or ggF+tth, and/or the partial decay width $\Gamma(h \to F)$, with $F = f_i\bar{f}_i$ or VV, are modified by r_{f_i}. SM denotes that the particular process is not modified. The total Higgs width Γ_h is modified by both modified Yukawa couplings.

The fact that a modification of λ_b affects not only $\Gamma(h \to b\bar{b})$ but also the total width, Γ_h, has a significant impact on the resulting LHC-allowed ring in the (T_R^b, T_I^b) plane, broadening it with respect to the case of a final state with a low branching ratio.

The constraint on T_R^b, T_I^b from the total Higgs width is comparable to but weaker than from eq. (5.14) for negative T_R^b, and significantly weaker for positive T_R^b. Therefore, it is not shown in figure 1.

5.2.3 λ_t

The Yukawa coupling λ_t is constrained by measurements of μ_{ggF}, μ_{tth} and $\mu_{\gamma\gamma}$. The latter provides a weaker constraint than the former two, so we do not use it. If the only modified Yukawa coupling is that of the top quark, then it is meaningful to combine the signal strengths of all of these top-mediated production processes, with all decays fixed to their SM values:

$$\mu_{\text{ggF}+t\bar{t}h} = 1.09 \pm 0.08\,, \tag{5.15}$$

which is dominated by the ggF process. For details see table 3. Using eq. (5.8) for $f = t$ and $\text{BR}_f = \text{BR}_g$, the remarkable precision of the experimental range (5.15) results in a narrow LHC-allowed ring in the (T_R^t, T_I^t) plane, see figure 2.

5.3 Two-flavor modification

In the presence of two dim-6 Yukawa terms, the modifications of Higgs production and/or decay can be grouped into the two categories detailed in table 1. The dependence of the signal strengths on the modified Yukawa interactions r_f and on the SM branching ratios is given by

$$\text{A:} \qquad \mu_{\text{SM}}^{f_1} = \mu_{f_1}^{\text{SM}} = \frac{r_{f_1}}{\Gamma_h/\Gamma_h^{\text{SM}}} = \frac{r_{f_1}}{1 + \text{BR}_{f_1}^{\text{SM}}(r_{f_1} - 1) + \text{BR}_{f_2}^{\text{SM}}(r_{f_2} - 1)}\,, \tag{5.16}$$

$$\text{B:} \qquad \mu_{f_1}^{f_2} = \frac{r_{f_1}\, r_{f_2}}{\Gamma_h/\Gamma_h^{\text{SM}}} = \frac{r_{f_1}\, r_{f_2}}{1 + \text{BR}_{f_1}^{\text{SM}}(r_{f_1} - 1) + \text{BR}_{f_2}^{\text{SM}}(r_{f_2} - 1)}\,, \tag{5.17}$$

JHEP05(2020)056

with $f_1, f_2 = \tau, b, t$ and where $\mathrm{BR}_t^{\mathrm{SM}} \equiv \mathrm{BR}_g^{\mathrm{SM}}$. Here the lower index of the signal strength μ denotes the modification of the Higgs production cross section whereas the upper index refers to the modification of the partial decay width, keeping in mind that the total Higgs width is modified by all modified Yukawa couplings.

In addition to the combinations A and B, we also evaluate the constraint from the total width itself with the dependence on r_f given in eq. (5.6). However, the present experimental bound on the total width [35] does not lead to a constraint on $T_I^{f_1,f_2}$ exceeding the constraints from the signal strengths of cases A and B.

When constraining dim-6 Yukawa couplings of two fermions f_1, f_2 simultaneously, we are dealing with four SMEFT parameters. As an example of these constraints, in what follows we set $T_R^{f_1,f_2} = 0$ and present the bounds in the $T_I^{f_1} - T_I^{f_2}$ plane. See appendix A.2 for details on how to obtain the corresponding limits.

5.3.1 λ_b and λ_τ

The production rates are neither affected by λ_b nor λ_τ. Thus, we can still use the experimental ranges of eq. (5.13) for $\mu_{\tau^+\tau^-}$ and eq. (5.14) for $\mu_{b\bar{b}}$. The theoretical expression for $\mu_{\tau^+\tau^-}$ and $\mu_{b\bar{b}}$ are, however, modified due to the modification of the total Higgs width by the two different Yukawa couplings, see eqs. (5.16), (A.1) and (A.2) with $f_1 = \tau, b$ and $f_2 = b, \tau$, respectively. The total Higgs width constrains $|T_I^b| \lesssim 0.6$, i.e. similar to the direct $h \to b\bar{b}$ bound, but not stronger. Therefore, the Γ_h bound is not shown in figure 3.

5.3.2 λ_t and λ_τ

For this combination of couplings, we use three relevant constraints:

$$\begin{aligned} \mu_{\mathrm{ggF}}^{\tau\tau} &= 0.99 \pm 0.44\,, \\ \mu_{\mathrm{VBF}+Vh}^{\tau\tau} &= 1.09 \pm 0.26\,, \\ \mu_{\mathrm{ggF}+tth}^{VV} &= 1.08 \pm 0.08\,, \end{aligned} \tag{5.18}$$

Because of the significantly higher precision of $\mu_{\mathrm{ggF}}^{\tau\tau}$ compared to $\mu_{tth}^{\tau\tau}$ (see table 2), we do not combine both production modes for the decay into $\tau\tau$, but use $\mu_{\mathrm{ggF}}^{\tau\tau}$. The theoretical expression for this channel is given by eq. (5.17) with $f_1 = t$, $f_2 = \tau$.

The combination of the t-independent production processes VBF and Vh, followed by the decay into $\tau^+\tau^-$, constrains T_I^τ with a mild dependence on T_I^t due to the modification of the total Higgs width, see eq. (5.16) with $f_1 = \tau$.

The opposite combination of Higgs production via λ_t and the decay into VV mainly constrains T_I^t with a mild dependence on T_I^τ via Γ_h. The structure of the signal strength μ_t^{VV} is given by eq. (5.16) with $f_1 = t$ and $f_2 = \tau$.

5.3.3 λ_t and λ_b

The combination of T_I^t and T_I^b is constrained by

$$\begin{aligned} \mu_{t\bar{t}h+ggF}^{b\bar{b}} &= 0.88 \pm 0.43\,, \\ \mu_{VH}^{bb} &= 0.98 \pm 0.15\,, \\ \mu_{\mathrm{ggF}+tth}^{VV} &= 1.08 \pm 0.08\,. \end{aligned} \tag{5.19}$$

JHEP05(2020)056

As μ^{bb}_{VBF} is not available at comparable precision, there is no need for a combination of VBF and Vh to constrain the b Yukawa coupling. The corresponding theoretical expressions are $\mu^{b\bar{b}}_{\text{ggF}+tth}$ according to eq. (5.17) with $f_1 = t$, $f_2 = b$, $\mu^{b\bar{b}}_{Vh}$ according to eq. (5.16) with $f_1 = b$, $f_2 = t$, and $\mu^{VV}_{\text{ggF}+tth}$ according to eq. (5.16) with $f_1 = t$, $f_2 = b$. The limits on (T^τ_I, T^b_I) resulting from μ^{bb}_{Vh} are weaker than from the other two experimental processes and are therefore not shown in figure 5.

6 Results

6.1 Single flavor modification

We present in this section the results of our combined analysis of three physical observables: Y_B, d_e and μ_f, from a single flavor source. We note the following points:

- Both the baryon asymmetry and the electron EDM are proportional to $(y_f/y_f^{SM})^2 T^f_I$, except for the top quark. This implies that, for a single CP violating source from $f \neq t$, contours of constant Y_B are also contours of constant d_e. In contrast, Y^t_B is approximately constant in T^t_R due to the large Yukawa coupling contributing to its thermal mass.
- The Y_B dependence on T^f_R is mild. Negative values of T_R generate a larger baryon asymmetry.
- The value $\mu_f = 1$ defines a circle in this plane through the SM point $T^f_I = T^f_R = 0$.
- Experimental bounds on μ_f constrain the dim-6 operators of each species to an annulus in the T^f_R, T^f_I plane.
- As all signal strengths μ_f are compatible with 1, the radius is approximately 0.25, where the exact value and the width of the ring depend on the precise bounds on μ_f and the value of BR^{SM}_f, see eq. (5.10). Hence the collider sensitivity on T^f_R and T^f_I reaches few times $\mathcal{O}(0.1)$.

6.1.1 λ_τ

The constraints on (T^τ_R, T^τ_I) are presented in figure 1 (left). The constraints on a complex Yukawa coupling for the tau-lepton from $\mu_{\tau^+\tau^-}$ and from d_e are comparable. While the EDM is more constraining on T^τ_I, the decay rate for $h \to \tau^+\tau^-$ restricts T^τ_R. Within the region allowed by the two measurements, there is a region where a complex λ_τ can generate enough CP violation to account for the observed BAU. The largest value of Y_B obtained in the allowed regions is

$$Y^{\tau,\text{max}}_B \simeq 2.4 Y^{\text{obs}}_B \,. \tag{6.1}$$

We quote this upper bound which is larger than Y^{obs}_B (and similar bounds further below) for three reasons:

- In our calculations, we use bubble wall parameters that are optimal for generating Y_B. The upper bound implies by how much these parameters can be less than optimal, and yet a complex λ_τ can provide the CP-violation necessary for baryogenesis.

JHEP05(2020)056

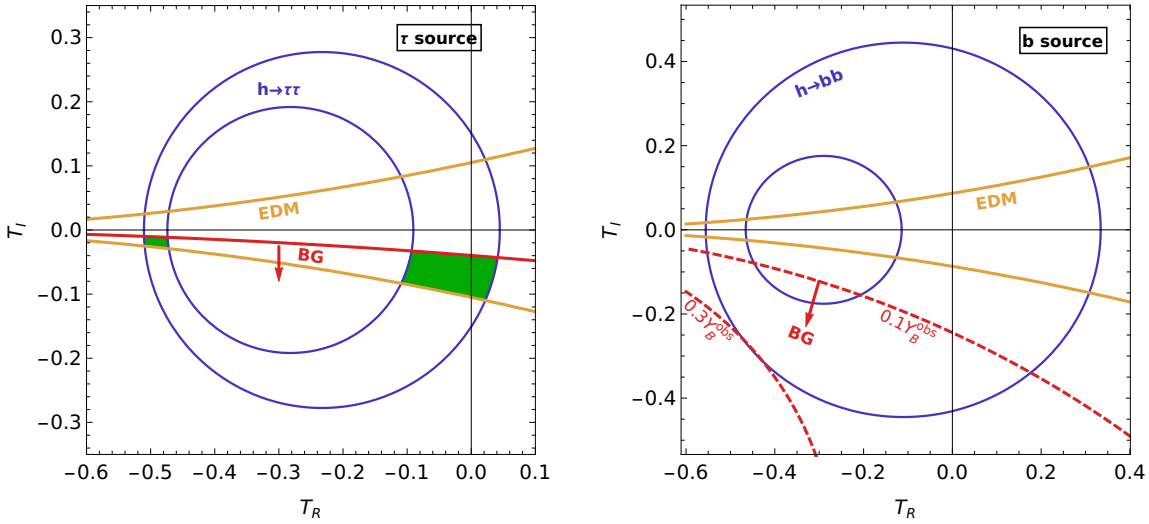

Figure 1. Constraints on (T_R^f, T_I^f), $f = \tau, b$, from $\mu_{f\bar{f}}$ (blue), d_e (yellow) and Y_B (red). Solid lines represent bounds, dashed red lines represent iso-Y_B curves within the bound. Regions allowed by all constraints are highlighted in green. *Left:* τ-lepton source, *right:* b-quark source.

- Similarly, the upper bound gives a sense for how sensitive our conclusions are with respect to uncertainties and approximations in the Y_B calculation.
- The upper bound is informative on which future experiments can test this scenario in a definitive way.

6.1.2 λ_b

The constraints on (T_R^b, T_I^b) are presented in figure 1 (right). Generating sufficient CP violation from a complex λ_b requires $|T_I^b| > 1$ (see eq. (3.5)). Therefore we conclude that λ_b cannot serve as the only source of CP violation to account for $Y_B^{\rm obs}$. While the $\mu_{b\bar{b}}$ constraint alone allows $Y_B^{(b)} \leq 0.33 Y_B^{\rm obs}$, the d_e constraint is stricter on T_I^b, leading to

$$Y_B^{(b)} \leq 0.04 Y_B^{\rm obs}. \tag{6.2}$$

6.1.3 λ_t

The constraints on (T_R^t, T_I^t) are presented in figure 2. The constraint on T_I^t from $\mu_{\rm ggF+tth}$ is three orders of magnitude weaker than from d_e. Thus, while the former by itself would allow for $Y_B^{(t)} \sim Y_B^{\rm obs}$, the latter restricts it:

$$Y_B^{(t)} \leq 0.02 Y_B^{\rm obs}. \tag{6.3}$$

The right plot presents a zoomed-in version of the figure to illustrate the strength of the EDM constraint, reducing the collider ring to two strips, one around the origin, and a narrow one around $T_R^t \simeq -0.5$. The latter translates to $\Lambda/\sqrt{X_R^t} \simeq v$, thus the EFT assumptions might not be fulfilled in this particular region of large negative T_R^t whereas

JHEP05(2020)056

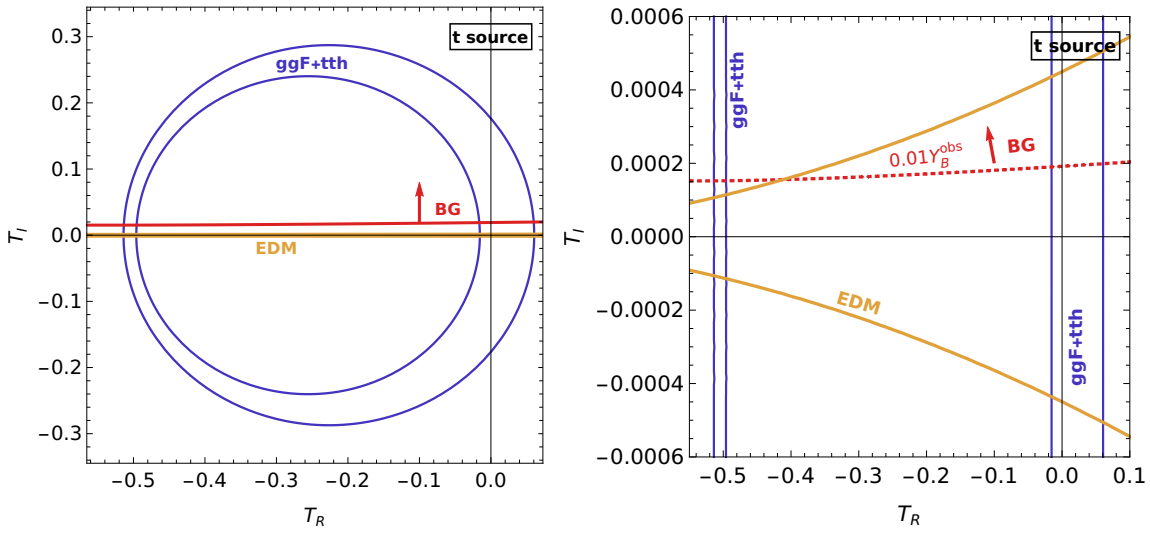

Figure 2. Top source: constraints on (T_R^t, T_I^t) from $\mu_{ggF+t\bar{t}h+th} = 1.09 \pm 0.08$ (blue), d_e (yellow) and Y_B (red). *Left:* full range of LHC bound, *right:* zoomed into range near EDM bound. The difference in the scaling of Y_B and d_e in this case is due to the non-negligible contribution of the Yukawa interactions to the thermal mass of the top.

the cutoff scale is well above v in the strip around the origin. The calculation of $Y_B^{(t)}$ is affected by larger uncertainties than in the τ- and b-cases due to the less suppressed higher-dimensional terms and the non-negligible higher-order effects in the VEV-insertion approximation [36]. Nevertheless, as our prediction of $Y_B^{(t)}$ is $\mathcal{O}(100)$ away from $Y_B^{\rm obs}$, our qualitative observation remains that the top quark does not induce sufficient baryon asymmetry.

6.2 Two flavor modification

In general, we expect that the dimension-six terms in the SMEFT would modify all Yukawa couplings. A combined contribution to the various observables from two or more flavors may open up new regions in the parameter space that can account for the baryon asymmetry. To understand this statement, consider eqs. (4.4) and (3.5). Given the fact that d_e and Y_B depend on different linear combinations of T_I^t, T_I^b and T_I^τ, there could be simultaneously cancellations between their contributions to d_e and enhancements of their contributions to Y_B. Our choice of $T_R^f = 0$ in the combination plots of two flavors represents a conservative case for the yield of Y_B.

6.2.1 λ_b and λ_τ

The constraints in the (T_I^τ, T_I^b) plane, for $T_R^\tau = T_R^b = 0$, are presented in figure 3. A much larger range of negative T_I^τ is consistent with $Y_B^{(\tau)} \gtrsim Y_B^{\rm obs}$. Here, T_I^b cancels against T_I^τ in d_e, and maintains $\mu_{\tau^+\tau^-}$ within bounds by increasing the total width, Γ_h. The maximal baryon asymmetry reached within the allowed range is

$$Y_B^{b+\tau,\max}(T_I^\tau = -0.4, T_I^b = +0.4) \simeq 7.8 Y_B^{\rm obs}\,. \tag{6.4}$$

JHEP05(2020)056

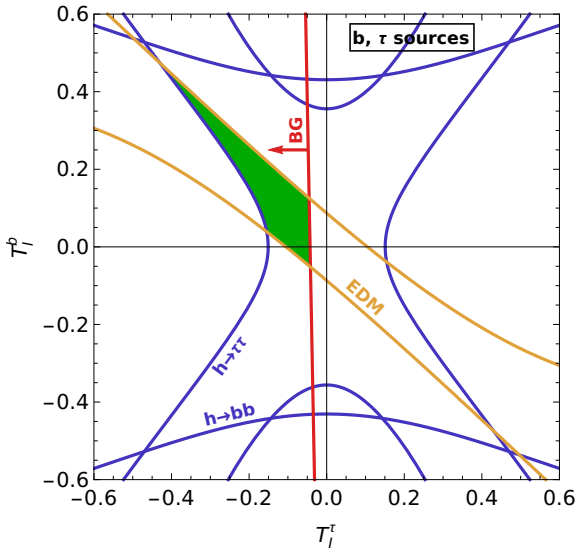

Figure 3. Constraints on b and τ sources with $T_R^{b,\tau} = 0$ from the LHC (blue), the eEDM (yellow) and Y_B (red). The parameter space allowed by all three constraints is highlighted in green. Collider range allowed by $\mu_{\tau^+\tau^-} = 0.91 \pm 0.13$ and $\mu_{b\bar{b}} = 1.02 \pm 0.14$, with μ_I^F given by equation (5.16).

6.2.2 λ_t and λ_τ

The constraints in the (T_I^τ, T_I^t) plane, for $T_R^\tau = T_R^t = 0$, are presented in figure 4. A much larger range of negative T_I^τ is consistent with $Y_B^{(\tau)} \gtrsim Y_B^{\rm obs}$. Here, T_I^t cancels against T_I^τ in d_e, and maintains $\mu_{\tau^+\tau^-}$ within bounds by decreasing the ggF and tth production rates. The maximal baryon asymmetry reached within the allowed range is

$$Y_B^{t+\tau,\max} = Y_B^{t+\tau}(T_I^\tau = -0.3, T_I^t = +0.0016) \simeq 6.4 Y_B^{\rm obs}\,. \tag{6.5}$$

6.2.3 λ_t and λ_b

The constraints in the (T_I^b, T_I^t) plane, for $T_R^b = T_R^t = 0$, are presented in figure 5. The LHC bounds on $\mu^{VV}_{\rm ggF+tth}$ in combination with the electron EDM constrain T_I^b to within a range such that

$$Y_B^{(t+b)} \lesssim 0.12 Y_B^{\rm obs}. \tag{6.6}$$

6.3 Obtaining $Y_B = Y_B^{\rm obs}$ with $d_e \simeq 0$ and $\mu_I^F \simeq 1$

Even if experiments strengthen the upper bound on d_e significantly, and narrow the allowed ranges around $\mu_I^F = 1$ in all modes, the possibility that our SMEFT framework accounts for the CP violation that is necessary for $Y_B = Y_B^{\rm obs}$ will remain viable.

To explain this statement, we go beyond the $T_R^f = 0$ examples of the previous subsections. Consider, for example, the case that both λ_τ and λ_b are modified by the dim-6 terms. We impose three constraints — $d_e = 0$, $\mu_{b\bar{b}} = 1$ and $\mu_{\tau^+\tau^-} = 1$ — on the four parameters $T_{I,R}^{b,\tau}$. It is always possible to choose a combination of T_I^τ and T_I^b such that $d_e = 0$, and corresponding values of T_R^τ and T_R^b such that $\mu_b = \mu_\tau = 1$. We therefore have one free parameter, bounded within some range of values, and we can check whether in

JHEP05(2020)056

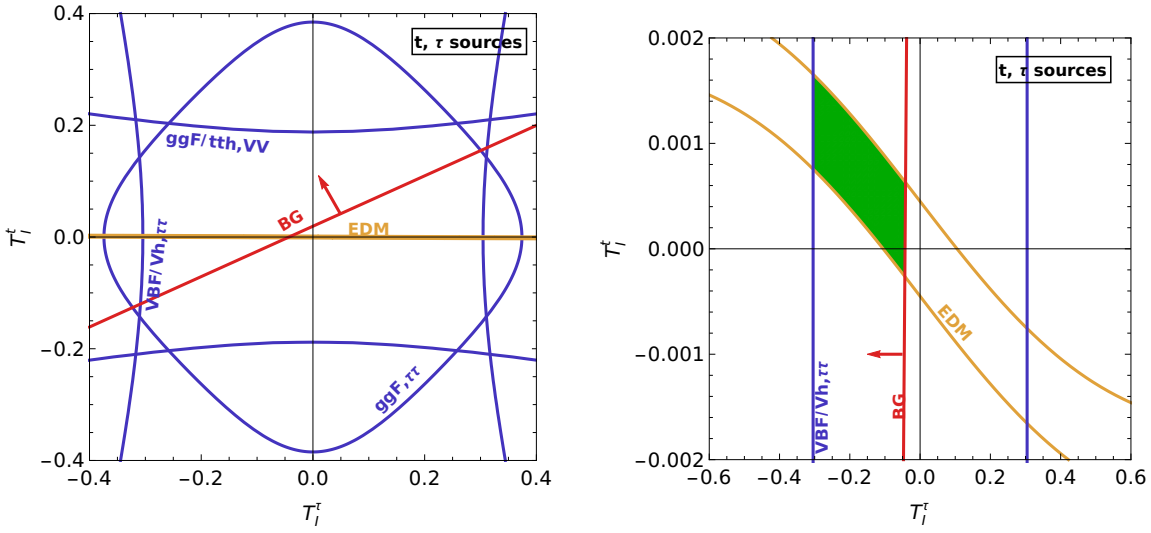

Figure 4. Constraints on t and τ sources with $T_R^{t,\tau} = 0$ from the LHC (blue), the eEDM (yellow) and Y_B (red). The parameter space allowed by all three constraints is highlighted in green. *Left:* full collider range allowed by $\mu^{\tau\tau}_{\rm ggF} = 0.99 \pm 0.44$ and $\mu^{\tau\tau}_{\rm VBF+Vh} = 1.09 \pm 0.26$ (combining ATLAS and CMS), *right:* zoomed into the EDM-allowed region.

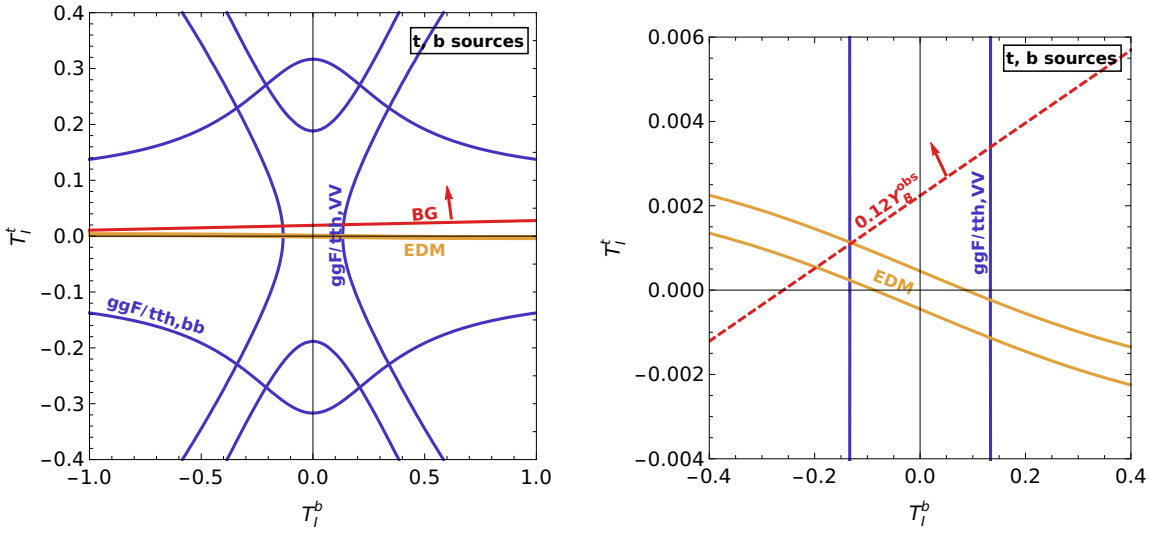

Figure 5. Constraints on t and b sources with $T_R^{t,b} = 0$ from the LHC (blue), the eEDM (yellow) and Y_B (red). *Left:* full collider range (combining ATLAS and CMS) allowed by $\mu^{bb}_{tth+ggF} = 0.88 \pm 0.43$ and $\mu^{VV}_{ggF+tth+th} = 1.08 \pm 0.08$, *right:* zoomed into the EDM-allowed region.

this range we can produce the observed baryon asymmetry. Using (4.4) and (5.16), we find that we can obtain up to

$$Y_B^{b+\tau,\max}(d_e = 0, \mu_b = \mu_\tau = 1) = 10.25 Y_B^{\rm obs}\,. \tag{6.7}$$

This corresponds to being very close to the point along the $\mu_\tau = 1$ circle that maximizes the baryon asymmetry, while the b only slightly reduces the produced baryon asymmetry.

JHEP05(2020)056

Indeed, simply maximizing the baryon asymmetry along $\mu_\tau = 1$ with $T_I^b = T_R^b = 0$ gives $Y_B^{(b+\tau),\max} = 10.33 Y_B^{\rm obs}$.

7 Conclusions

We studied in detail aspects of CP violation in the SMEFT. Specifically, we considered dimension-six terms involving the Higgs field and the third generation fermion fields, and analyzed the consequences for electroweak baryogenesis, for the electric dipole moment of the electron, and for Higgs production and decay rates. There is an interesting interplay between the three constraints. Our main conclusions are the following:

- A complex Yukawa coupling of the tau-lepton can provide large enough CP violation to account for the baryon asymmetry.
- A complex Yukawa coupling of neither the top-quark quark nor the bottom-quark can provide large enough CP violation to account for the baryon asymmetry: $Y_B^{(t)} \lesssim 0.02 Y_B^{\rm obs}$ and $Y_B^{(b)} \lesssim 0.04 Y_B^{\rm obs}$.
- The reason why the tau-lepton is more successful than the bottom- or the top-quark is that the strong sphalerons do not act on the tau-lepton. Therefore, the asymmetry created by a complex tau-Yukawa coupling is not washed out as strongly as the one of the quarks. Furthermore, the large leptonic diffusion coefficients, see eq. (B.3), enable an efficient diffusion of the asymmetry into the broken phase. These effects overcompensate the smaller, but still sizeable, τ-Yukawa coupling.
- Limited by the upper bound on $\mu_{\mu^+\mu^-}$, a complex Yukawa coupling of the muon can account for $0.16 Y_B^{\rm obs}$ [14], i.e. for more than the third-generations quarks, due to the advantages of leptons as for the τ despite the smaller $y_\mu^{\rm SM}$. Even a future measurement of $\mu_{\mu^+\mu^-} = 1$ would allow for $0.12 Y_B^{\rm obs}$, which remains more than from t or b.
- There can be substantial cancellations between the contributions of the third generation fermions to d_e, that are not necessarily accompanied by cancellations in their contributions to Y_B. In fact, one can have:
  - $d_e^{(b+\tau)} = 0$ simultaneously with $Y_B^{(b+\tau)} \sim Y_B^{\rm obs}$;
  - $d_e^{(t+\tau)} = 0$ simultaneously with $Y_B^{(t+\tau)} \sim Y_B^{\rm obs}$;
  - $d_e^{(t+b)} = 0$ simultaneously with $Y_B^{(t+b)} \sim 0.12 Y_B^{\rm obs}$.

  In other words, we can have successful electroweak baryogenesis without having a signal for the electron dipole moment of the electron.
- Such cancellations allow T_I^τ to further increase $Y_B^{(\tau)} > Y_B^{\rm obs}$. Consequently, near-future measurements of d_e or $\mu_{\tau^+\tau^-}$ are unlikely to exclude the scenario of τ-driven electroweak baryogenesis.

JHEP05(2020)056

- In fact, even if future experimental measurements establish $d_e \simeq 0$ and $\mu_I^F \simeq 1$ in all relevant modes, the scenario where a complex λ_τ provides the CP violation that is necessary for baryogenesis will not be excluded.

- Measuring CP violation in the decays of $h \to \tau^+\tau^-$ is crucial to determine the viability of baryogenesis in this SMEFT framework with dimension six couplings.

For a complex λ_τ to account for $Y_B^{\rm obs}$, T_I^τ in the range $0.01 - 0.1$ is required. This can be translated via $T_I^\tau \equiv (v^2/2\Lambda^2)(X_I^\tau/y_\tau)$ into a upper bound,

$$\Lambda/\sqrt{X_I^\tau} \lesssim 18 \text{ TeV } (0.01/T_I^\tau)^{1/2}. \tag{7.1}$$

Our work is largely consistent with refs. [13, 17]. We extended previous results to consider non-negligible values of T_R^f which enlarges the available parameter space and provides a more complex interplay among the different fermion species when applying the constraints from EDMs and Higgs physics results from colliders. Moreover, we consider also the cases that two third generation fermions contribute to the CP violation, and find that even if experiments find no deviations from the SM predictions, large enough Y_B can be generated in the SMEFT.

It is interesting to note that, while d_e and Y_B sum over the contributions of all Yukawa couplings, the ATLAS and CMS measurements of μ_I^F are flavor specific. Moreover, a dedicated search for CP violation in the decay $h \to f\bar{f}$ is unique in allowing a separate investigation of the imaginary part of each Yukawa coupling λ_f.

We have shown that the τ interactions are the only stand-alone option for generating the matter-antimatter asymmetry of the Universe. This situation implies that a significant step in probing the CP violation aspect of electroweak baryogenesis in the SMEFT framework can be achieved by searching for CP violation in $h \to \tau^+\tau^-$ decays. Thus, CP violation properties of the τ-lepton interactions should be a priority experimentally as this could provide the most significant constraints on the viability of electroweak baryogenesis in the context of the SMEFT framework.

In the future it will be important to further improve the sensitivity to a possible CP-odd component of this coupling at the LHC and future colliders, and to evaluate the baryon asymmetry corresponding to the constrained amount of CP-violation. An experimental HL-LHC projection [37] and several phenomenological analyses [38–41] have already been performed in this direction. Machine Learning (ML) may also play a useful role in further scrutinizing the CP nature of the Higgs-τ interaction [42, 43]. In addition, CP analyses of the t-Higgs coupling have been proposed, including ML [44–46].

Acknowledgments

We are grateful to Jorinde van de Vis for very helpful discussions. We thank Daniel Aloni for interesting discussions during the early stage of this work and the Fermilab and Cornell theory seminar audiences for stimulating comments. ML would like to deeply thank the Weizmann Institute of Science for its hospitality during the completion of this work. EF

JHEP05(2020)056

channel	experiment	$\sqrt{s}$/ TeV	$\mathscr{L}$/ fb^{-1}	comment	μ	Ref.
$h \to \tau^+\tau^-$	ATLAS+CMS	7+8	$5 + 20$		$1.11^{+0.24}_{-0.22}$	[3]
	ATLAS	13	36.1	ggF, VBF	$1.09^{+0.35}_{-0.30}$	[47]
	CMS	13	77	ggF, $\bar{b}b$, VBF, Vh	0.75 ± 0.17	[48]
	ATLAS+CMS	7+8+13		all prod., priv. comb.	0.91 ± 0.13	[3, 47, 48]
$h \to \mu^+\mu^-$	ATLAS	13	139	upper bound at 95% C. L.	< 1.7	[49]
	CMS		35.9		< 2.9	[50]
$h \to \bar{b}b$	ATLAS	13	79.8	VBF+VH	1.23 ± 0.26	[4]
				$t\bar{t}h + th$	$0.79^{+0.60}_{-0.59}$	
	CMS	7+8+13	41.3	VH (0-2ℓ, 2 b-tags+jets)	1.01 ± 0.22	[51]
				all prod.	1.04 ± 0.2	
	ATLAS+CMS	7+8+13		VH, priv. comb.	0.98 ± 0.15	[51, 52]
				all prod., priv. comb.	1.02 ± 0.14	

Table 2. Collider limits on the Higgs signal strengths involving the τ, μ and b. In our private combinations, the uncertainties are approximated as symmetric.

was supported by the Minerva Foundation. YN is the Amos de-Shalit chair of theoretical physics, and is supported by grants from the Israel Science Foundation (grant number 394/16), the United States-Israel Binational Science Foundation (BSF), Jerusalem, Israel (grant number 2014230), and the Yeda-Sela (YeS) Center for Basic Research.

A Collider limits

A.1 Experimental bounds

Tables 2 and 3 contain the details of the collider limits from Higgs physics, by both CMS and ATLAS, that have been used to constrain the Higgs signal strengths for all third generation fermions.

A.2 Analytical bounds for $T_R^f = 0$

When we consider simultaneous modifications of two Yukawa couplings in figures 3–5, we take as an example the case of $T_R^f = 0$. Here we provide the conditions on the relations between $\mathrm{BR}_f^{\mathrm{SM}}$ and the experimental bounds on μ_I^F under which a bound on $T_I^{f_1}$, $T_I^{f_2}$ arises in the two possible cases presented in table 1.

Case A. If either the production or the decay is not modified with respect to the SM (namely VBF/Vh production or the decay $h \to VV$), the signal strength is given by eq. (5.16). Depending on whether the measured signal rate is $\mu_{f_1} >$ or < 1, the resulting exclusion contour has an asymptote at

$$T_I^{f_1,\mathrm{asymp}} = \pm\sqrt{\frac{1-\mu_{f_1}}{\mu_{f_1}(1+8\mathrm{BR}_{f_1}^{\mathrm{SM}})-9}}\,, \quad \text{if } \frac{9}{1+8\mathrm{BR}_{f_1}^{\mathrm{SM}}} > \mu_{f_1} > 1\,, \tag{A.1}$$

$$T_I^{f_2,\mathrm{asymp}} = \pm\sqrt{\frac{1-\mu_{f_1}}{\mu_{f_1}(1+8\mathrm{BR}_{f_2}^{\mathrm{SM}})-1}}\,, \quad \text{if } \frac{1}{1+8\mathrm{BR}_{f_2}^{\mathrm{SM}}} < \mu_{f_1} < 1\,. \tag{A.2}$$

JHEP05(2020)056

channel	experiment	$\sqrt{s}$/ TeV	$\mathscr{L}$/ fb^{-1}	comment	μ	Ref.
ggF	ATLAS	13	≤ 79.8	$H \to \gamma\gamma$	0.96 ± 0.14	[4]
				$H \to \tau\tau$	$0.96^{+0.59}_{-0.52}$	
				all decays, fixed to SM	1.04 ± 0.09	
	CMS	13	35.9	$H \to \gamma\gamma$	$1.16^{+0.30}_{-0.25}$	[5]
				$H \to \tau\tau$	$1.05^{+0.75}_{-0.67}$	
				all decays, fixed to SM	$1.22^{+0.20}_{-0.18}$	
	ATLAS+CMS	13		$H \to \gamma\gamma$, priv. comb.	1.00 ± 0.12	[4, 5]
				$H \to \tau\tau$, priv. comb.	0.99 ± 0.44	
				all decays SM, priv. comb.	1.07 ± 0.08	
$\bar{t}th + th$	ATLAS	13	≤ 79.8	$H \to \gamma\gamma$	$1.1^{+0.41}_{-0.35}$	[4]
				$H \to \tau\tau$	$1.38^{+1.13}_{-0.96}$	
				$H \to \bar{b}b$	$0.79^{+0.60}_{-0.59}$	
				all decays, fixed to SM	$1.21^{+0.26}_{-0.24}$	
	CMS	13	35.9	$H \to \gamma\gamma$	$2.18^{+1.25}_{-1.06}$	[5]
				$H \to \tau\tau$	$0.23^{+1.46}_{-1.24}$	
				$H \to \bar{b}b$	$0.91^{+0.64}_{-0.61}$	
				all decays, fixed to SM	$1.18^{+0.43}_{-0.38}$	
	ATLAS+CMS	13		$H \to \gamma\gamma$, priv. comb.	1.21 ± 0.36	[4, 5]
				$H \to \tau\tau$, priv. comb.	0.95 ± 0.83	
				$H \to \bar{b}b$, priv. comb.	0.87 ± 0.43	
				all decays SM, priv. comb.	1.20 ± 0.21	
ggF+$\bar{t}th + \bar{t}H$	ATLAS+CMS	13		all decays SM, priv. comb.	1.09 ± 0.08	[4, 5]
				$h \to VV$, priv. comb.	1.08 ± 0.08	
$h \to \gamma\gamma$	ATLAS	13	138	tth	$1.38^{+0.41}_{-0.36}$	[53, 54]
	CMS		77.4		$1.7^{+0.6}_{-0.5}$	[53, 55]
	ATLAS		≤ 79.8	priv. comb. of all prod.	1.02 ± 0.12	[4]
	CMS		35.9	SM ratio of production modes	$1.2^{+0.25}_{-0.20}$	[5]

Table 3. Collider limits on the Higgs signal strengths involving the t. In our private combinations, the uncertainties are approximated as symmetric. The $h \to \gamma\gamma$ decay does not lead to competitive bounds on T^t_R, T^t_I.

For example, the 2σ lower bound on $\mu^{\tau\tau}_{\text{VBF}+Vh}$ of 0.57 is smaller than $1/(1+8\text{BR}^{\text{SM}}_g) = 0.59$, see eq. (A.2). Therefore, this lower bound does not imply a limit on T^τ_I, T^t_I in figure 4, but a slight experimental improvement will give rise to a limit. A measurement of $\mu_{f_1} = 1$ results in an X-shaped contour crossing through the origin $\left(T^{f_1}_I, T^{f_2}_I\right) = (0,0)$.

Case B. The production via the coupling λ_{f_1} (hence λ_t) and the decay $h \to f_2\bar{f}_2$, while the total width is modified by both λ_{f_1} and λ_{f_2}, are described by the signal strength in eq. (5.17). It results in a bound if

$$1 \leq \mu^{f_2}_{f_1} \leq \frac{9}{1+8\text{BR}^{\text{SM}}_{f_1}}, \frac{9}{1+8\text{BR}^{\text{SM}}_{f_2}}\,. \tag{A.3}$$

JHEP05(2020)056

For $\mu_{f_1}^{f_2} < 1$ there is no real solution. Consequently, the lower bound on $\mu_{\text{ggF}}^{\tau\tau}$ does not yield a limit in the T_I^τ-T_I^t plane. In case $\mu_{f_1}^{f_2} = 1$ is measured, the only solution is the trivial one, namely the SM prediction of $T_I^\tau = T_I^t = 0$, or the physically impossible case of $\text{BR}_g^{\text{SM}} = \text{BR}_\tau^{\text{SM}} = 1$.

B Benchmark values for baryogenesis calculations

In this appendix we present benchmark values for various parameters required to reproduce our results. Further expressions and details can be found in [27]. We take the nucleation temperature to be $T_N = 88\,\text{GeV}$. At this temperature, the gauge couplings and Higgs VEV are [13]

$$g' = 0.36\,, \qquad g = 0.65\,, \qquad g_s = 1.23\,, \qquad v_N = 152\,\text{GeV}\,. \tag{B.1}$$

The entropy density, written in terms of the temperature and the entropy degrees of freedom g^*, is given by [13]

$$s = \frac{2\pi^2}{45} g^* T_N^3\,, \quad g^* = 106.75. \tag{B.2}$$

The bubble wall velocity and width are taken from [17], with values

$$v_w = 0.05\,, \quad L_w = 0.11\,\text{GeV}^{-1}\,,$$

respectively. We apply the VEV-insertion approximation as well as the diffusion approximation. The diffusion coefficients are approximately given by [56, 57]

$$D_{l_R} = 380/T\,, \qquad D_{l_L} = 100/T\,, \qquad D_u = D_d = D_q = 6/T\,, \qquad D_h = 100/T\,. \tag{B.3}$$

The thermal widths are [58]

$$\Gamma_{\text{lepton}} \approx 0.002T\,, \quad \Gamma_{\text{quark.}} \approx 0.16T\,. \tag{B.4}$$

Finally, the sphaleron rates are given by [59, 60]

$$\Gamma_{\text{ws}}(z) = 120\alpha_w^5 T_N \Theta(z<0)\,, \quad \Gamma_{\text{ss}} = 14\alpha_s^4 T_N\,. \tag{B.5}$$

Open Access. This article is distributed under the terms of the Creative Commons Attribution License (CC-BY 4.0), which permits any use, distribution and reproduction in any medium, provided the original author(s) and source are credited.

References

[1] ATLAS collaboration, *Observation of a new particle in the search for the Standard Model Higgs boson with the ATLAS detector at the LHC*, *Phys. Lett.* **B 716** (2012) 1 [arXiv:1207.7214] [INSPIRE].

[2] CMS collaboration, *Observation of a New Boson at a Mass of 125 GeV with the CMS Experiment at the LHC*, *Phys. Lett.* **B 716** (2012) 30 [arXiv:1207.7235] [INSPIRE].

JHEP05(2020)056

[3] ATLAS and CMS collaborations, *Measurements of the Higgs boson production and decay rates and constraints on its couplings from a combined ATLAS and CMS analysis of the LHC pp collision data at $\sqrt{s} = 7$ and 8 TeV*, *JHEP* **08** (2016) 045 [arXiv:1606.02266] [INSPIRE].

[4] ATLAS collaboration, *Combined measurements of Higgs boson production and decay using up to 80 fb^{-1} of proton-proton collision data at $\sqrt{s} = 13$ TeV collected with the ATLAS experiment*, *Phys. Rev.* **D 101** (2020) 012002 [arXiv:1909.02845] [INSPIRE].

[5] CMS collaboration, *Combined measurements of Higgs boson couplings in proton-proton collisions at $\sqrt{s} = 13$ TeV*, *Eur. Phys. J.* **C 79** (2019) 421 [arXiv:1809.10733] [INSPIRE].

[6] LHC Higgs Cross Section Working Group collaboration, *Handbook of LHC Higgs Cross Sections: 4. Deciphering the Nature of the Higgs Sector*, arXiv:1610.07922 [INSPIRE].

[7] P. Bechtle, S. Heinemeyer, O. Stål, T. Stefaniak and G. Weiglein, *Probing the Standard Model with Higgs signal rates from the Tevatron, the LHC and a future ILC*, *JHEP* **11** (2014) 039 [arXiv:1403.1582] [INSPIRE].

[8] J. Ellis, C.W. Murphy, V. Sanz and T. You, *Updated Global SMEFT Fit to Higgs, Diboson and Electroweak Data*, *JHEP* **06** (2018) 146 [arXiv:1803.03252] [INSPIRE].

[9] CMS collaboration, *Searches for physics beyond the standard model with the M_{T2} variable in hadronic final states with and without disappearing tracks in proton-proton collisions at $\sqrt{s} = 13$ TeV*, *Eur. Phys. J.* **C 80** (2020) 3 [arXiv:1909.03460] [INSPIRE].

[10] ATLAS collaboration, *Search for new resonances in mass distributions of jet pairs using 139 fb^{-1} of pp collisions at $\sqrt{s} = 13$ TeV with the ATLAS detector*, *JHEP* **03** (2020) 145 [arXiv:1910.08447] [INSPIRE].

[11] W. Buchmüller and D. Wyler, *CP Violation and R Invariance in Supersymmetric Models of Strong and Electroweak Interactions*, *Phys. Lett.* **121B** (1983) 321 [INSPIRE].

[12] B. Grzadkowski, M. Iskrzynski, M. Misiak and J. Rosiek, *Dimension-Six Terms in the Standard Model Lagrangian*, *JHEP* **10** (2010) 085 [arXiv:1008.4884] [INSPIRE].

[13] J. de Vries, M. Postma, J. van de Vis and G. White, *Electroweak Baryogenesis and the Standard Model Effective Field Theory*, *JHEP* **01** (2018) 089 [arXiv:1710.04061] [INSPIRE].

[14] E. Fuchs, M. Losada, Y. Nir and Y. Viernik, *Implications of the Upper Bound on $h \to \mu^+\mu^-$ on the Baryon Asymmetry of the Universe*, *Phys. Rev. Lett.* **124** (2020) 181801 [arXiv:1911.08495] [INSPIRE].

[15] A. Kobakhidze, L. Wu and J. Yue, *Electroweak Baryogenesis with Anomalous Higgs Couplings*, *JHEP* **04** (2016) 011 [arXiv:1512.08922] [INSPIRE].

[16] H.-K. Guo, Y.-Y. Li, T. Liu, M. Ramsey-Musolf and J. Shu, *Lepton-Flavored Electroweak Baryogenesis*, *Phys. Rev.* **D 96** (2017) 115034 [arXiv:1609.09849] [INSPIRE].

[17] J. De Vries, M. Postma and J. van de Vis, *The role of leptons in electroweak baryogenesis*, *JHEP* **04** (2019) 024 [arXiv:1811.11104] [INSPIRE].

[18] S. Jana and S. Nandi, *New Physics Scale from Higgs Observables with Effective Dimension-6 Operators*, *Phys. Lett.* **B 783** (2018) 51 [arXiv:1710.00619] [INSPIRE].

[19] J. Brod, U. Haisch and J. Zupan, *Constraints on CP-violating Higgs couplings to the third generation*, *JHEP* **11** (2013) 180 [arXiv:1310.1385] [INSPIRE].

[20] Particle Data Group collaboration, *Review of Particle Physics*, *Phys. Rev.* **D 98** (2018) 030001 [INSPIRE].

JHEP05(2020)056

[21] M.B. Gavela, P. Hernández, J. Orloff and O. Pene, *Standard model CP-violation and baryon asymmetry*, *Mod. Phys. Lett.* **A 9** (1994) 795 [hep-ph/9312215] [INSPIRE].

[22] P. Huet and E. Sather, *Electroweak baryogenesis and standard model CP-violation*, *Phys. Rev.* **D 51** (1995) 379 [hep-ph/9404302] [INSPIRE].

[23] K. Kajantie, M. Laine, K. Rummukainen and M.E. Shaposhnikov, *Is there a hot electroweak phase transition at $m_H \gtrsim m_W$?*, *Phys. Rev. Lett.* **77** (1996) 2887 [hep-ph/9605288] [INSPIRE].

[24] F. Csikor, Z. Fodor and J. Heitger, *Endpoint of the hot electroweak phase transition*, *Phys. Rev. Lett.* **82** (1999) 21 [hep-ph/9809291] [INSPIRE].

[25] C. Lee, V. Cirigliano and M.J. Ramsey-Musolf, *Resonant relaxation in electroweak baryogenesis*, *Phys. Rev.* **D 71** (2005) 075010 [hep-ph/0412354] [INSPIRE].

[26] G.A. White, *A Pedagogical Introduction to Electroweak Baryogenesis*, Morgan & Claypool Publishers (2016) [DOI].

[27] E. Fuchs, M. Losada, Y. Nir and Y. Viernik, *Analytic techniques for solving the transport equations in electroweak baryogenesis*, in preparation.

[28] ACME collaboration, *Improved limit on the electric dipole moment of the electron*, *Nature* **562** (2018) 355 [INSPIRE].

[29] G. Panico, A. Pomarol and M. Riembau, *EFT approach to the electron Electric Dipole Moment at the two-loop level*, *JHEP* **04** (2019) 090 [arXiv:1810.09413] [INSPIRE].

[30] V. Cirigliano, W. Dekens, J. de Vries and E. Mereghetti, *Constraining the top-Higgs sector of the Standard Model Effective Field Theory*, *Phys. Rev.* **D 94** (2016) 034031 [arXiv:1605.04311] [INSPIRE].

[31] J. Brod and E. Stamou, *Electric dipole moment constraints on CP-violating heavy-quark Yukawas at next-to-leading order*, arXiv:1810.12303 [INSPIRE].

[32] K. Fuyuto, W.-S. Hou and E. Senaha, *Cancellation mechanism for the electron electric dipole moment connected with the baryon asymmetry of the Universe*, *Phys. Rev.* **D 101** (2020) 011901 [arXiv:1910.12404] [INSPIRE].

[33] nEDM collaboration, *Measurement of the permanent electric dipole moment of the neutron*, *Phys. Rev. Lett.* **124** (2020) 081803 [arXiv:2001.11966] [INSPIRE].

[34] LHCPhysics, *SM Higgs Branching Ratios and Total Decay Widths (update in CERN Report4 2016)*, https://twiki.cern.ch/twiki/bin/view/LHCPhysics/CERNYellowReportPageBR.

[35] CMS collaboration, *Measurements of the Higgs boson width and anomalous HVV couplings from on-shell and off-shell production in the four-lepton final state*, *Phys. Rev.* **D 99** (2019) 112003 [arXiv:1901.00174] [INSPIRE].

[36] M. Postma and J. Van De Vis, *Source terms for electroweak baryogenesis in the vev-insertion approximation beyond leading order*, *JHEP* **02** (2020) 090 [arXiv:1910.11794] [INSPIRE].

[37] ATLAS collaboration, *Probing the $\mathcal{CP}$ nature of the Higgs boson coupling to τ leptons at HL-LHC*, ATL-PHYS-PUB-2019-008.

[38] R. Harnik, A. Martin, T. Okui, R. Primulando and F. Yu, *Measuring CP-violation in $h \to \tau^+\tau^-$ at Colliders*, *Phys. Rev.* **D 88** (2013) 076009 [arXiv:1308.1094] [INSPIRE].

[39] S. Berge, W. Bernreuther and S. Kirchner, *Determination of the Higgs CP-mixing angle in the tau decay channels at the LHC including the Drell-Yan background*, *Eur. Phys. J.* **C 74** (2014) 3164 [arXiv:1408.0798] [INSPIRE].

JHEP05(2020)056

[40] K. Hagiwara, K. Ma and S. Mori, *Probing CP-violation in $h \to \tau^- \tau^+$ at the LHC*, *Phys. Rev. Lett.* **118** (2017) 171802 [arXiv:1609.00943] [INSPIRE].

[41] X. Chen and Y. Wu, *Probing the CP-Violation effects in the $h\tau\tau$ coupling at the LHC*, *Phys. Lett.* **B 790** (2019) 332 [arXiv:1708.02882] [INSPIRE].

[42] E. Richter-Was and Z. Was, *LHC Higgs CP Sensitive Observables in $H \to \tau^+\tau^-$; $\tau^\pm \to (3\pi)^\pm \nu$ and Machine Learning Benefits*, in *54th Rencontres de Moriond on QCD and High Energy Interactions (Moriond QCD 2019)*, La Thuile, Italy, 23–30 March 2019 (2019) [arXiv:1905.05523] [INSPIRE].

[43] K. Lasocha, E. Richter-Was, M. Sadowski and Z. Was, *Deep Neural Network application: Higgs boson CP state mixing angle in $H \to \tau\tau$ decay and at LHC*, arXiv:2001.00455 [INSPIRE].

[44] J. Ren, L. Wu and J.M. Yang, *Unveiling CP property of top-Higgs coupling with graph neural networks at the LHC*, *Phys. Lett.* **B 802** (2020) 135198 [arXiv:1901.05627] [INSPIRE].

[45] C. Englert, P. Galler, A. Pilkington and M. Spannowsky, *Approaching robust EFT limits for CP-violation in the Higgs sector*, *Phys. Rev.* **D 99** (2019) 095007 [arXiv:1901.05982] [INSPIRE].

[46] D.A. Faroughy, J.F. Kamenik, N. Košnik and A. Smolkovič, *Probing the CP nature of the top quark Yukawa at hadron colliders*, *JHEP* **02** (2020) 085 [arXiv:1909.00007] [INSPIRE].

[47] ATLAS collaboration, *Cross-section measurements of the Higgs boson decaying into a pair of τ-leptons in proton-proton collisions at $\sqrt{s} = 13$ TeV with the ATLAS detector*, *Phys. Rev.* **D 99** (2019) 072001 [arXiv:1811.08856] [INSPIRE].

[48] CMS collaboration, *Measurement of Higgs boson production and decay to the $\tau\tau$ final state*, CMS-PAS-HIG-18-032.

[49] ATLAS collaboration, *A search for the dimuon decay of the Standard Model Higgs boson in pp collisions at $\sqrt{s} = 13$ TeV with the ATLAS Detector*, ATLAS-CONF-2019-028.

[50] CMS collaboration, *Search for the Higgs boson decaying to two muons in proton-proton collisions at $\sqrt{s} = 13$ TeV*, *Phys. Rev. Lett.* **122** (2019) 021801 [arXiv:1807.06325] [INSPIRE].

[51] CMS collaboration, *Observation of Higgs boson decay to bottom quarks*, *Phys. Rev. Lett.* **121** (2018) 121801 [arXiv:1808.08242] [INSPIRE].

[52] ATLAS collaboration, *Observation of $H \to b\bar{b}$ decays and VH production with the ATLAS detector*, *Phys. Lett.* **B 786** (2018) 59 [arXiv:1808.08238] [INSPIRE].

[53] J.S. Keller, *Measurements of ttH and tH production at ATLAS + CMS*, ATL-PHYS-SLIDE-2019-291.

[54] ATLAS collaboration, *Measurement of Higgs boson production in association with a $t\bar{t}$ pair in the diphoton decay channel using 139 fb^{-1} of LHC data collected at $\sqrt{s} = 13$ TeV by the ATLAS experiment*, ATLAS-CONF-2019-004.

[55] CMS collaboration, *Measurement of the associated production of a Higgs boson and a pair of top-antitop quarks with the Higgs boson decaying to two photons in proton-proton collisions at $\sqrt{s} = 13$ TeV*, CMS-PAS-HIG-18-018.

[56] M. Joyce, T. Prokopec and N. Turok, *Nonlocal electroweak baryogenesis. Part 1: Thin wall regime*, *Phys. Rev.* **D 53** (1996) 2930 [hep-ph/9410281] [INSPIRE].

JHEP05(2020)056

[57] J.M. Cline, M. Joyce and K. Kainulainen, *Supersymmetric electroweak baryogenesis*, *JHEP* **07** (2000) 018 [hep-ph/0006119] [INSPIRE].

[58] P. Elmfors, K. Enqvist, A. Riotto and I. Vilja, *Damping rates in the MSSM and electroweak baryogenesis*, *Phys. Lett.* **B 452** (1999) 279 [hep-ph/9809529] [INSPIRE].

[59] D. Bödeker, G.D. Moore and K. Rummukainen, *Chern-Simons number diffusion and hard thermal loops on the lattice*, *Phys. Rev.* **D 61** (2000) 056003 [hep-ph/9907545] [INSPIRE].

[60] G.D. Moore and M. Tassler, *The Sphaleron Rate in* SU(N) *Gauge Theory*, *JHEP* **02** (2011) 105 [arXiv:1011.1167] [INSPIRE].

JHEP05(2020)056